Surface & Coatings Technology 303 (2016) 372–384

Contents lists available at ScienceDirect

Surface & Coatings Technology

journal homepage: www.elsevier.com/locate/surfcoat

Influence of the addition of SiO_2 nanoparticles to a hybrid coating applied on an AZ31 alloy for early corrosion protection

R.N. Peres [a], E.S.F. Cardoso [a], M.F. Montemor [b], H.G. de Melo [c], A.V. Benedetti [d], P.H. Suegama [a,*]

[a] Faculdade de Ciências Exatas e Tecnologia, Universidade Federal da Grande Dourados, Rodovia Dourados — Itahum, km 12, P.O. Box 364, 9804-970 Dourados, MS, Brazil
[b] CQE, Instituto Superior Técnico, Universidade de Lisboa, Av. Rovisco Pais, 1049-001 Lisboa, Portugal
[c] Departamento de Eng. Metalúrgica e de Materiais, Escola Politécnica da Universidade de São Paulo, Av. Prof. Mello Moraes n. 2463, 05508-030 São Paulo, SP, Brazil
[d] Departamento Físico-Química, Instituto de Química, Universidade Estadual Paulista, UNESP, P.O 355, 14801-970 Araraquara, SP, Brazil

ARTICLE INFO

Article history:
Received 5 May 2015
Revised 14 December 2015
Accepted in revised form 16 December 2015
Available online 19 December 2015

Keywords:
AZ31 alloy
Hybrid coating
EIS
Morphological characterization

ABSTRACT

This work aims to investigate the corrosion resistance of AZ31 magnesium alloy protected by hybrid films based on tetraethylorthosilane (TEOS) and (3-glycidoxypropyl)trimethoxysilane (GPTMS) with the addition of different amounts of SiO_2 nanoparticles. The electrochemical techniques used to evaluate the corrosion resistance in 0.1 mol l^{l-1} NaCl electrolyte were open circuit potential (EOC) measurements and electrochemical impedance spectroscopy (EIS), which diagrams were fitted using equivalent electrical circuits (EEC). Surface and cross-section analyses of the bare and coated samples were performed by means of scanning electron microscopy (SEM) and energy dispersive spectroscopy (EDS) before and after electrochemical studies. The results showed that the coatings protected the Mg alloy against corrosion, and that the addition of the nanoparticles improves the corrosion resistance. The morphological characterization showed, for the coated systems, the presence of corrosion products adhered to the metal surface, a process that seems to be hindered in the presence of the SiO_2 nanoparticles. The results demonstrate that an optimum amount of nanoparticles must be added to the coating in order to optimize the anticorrosion protection and that only early stages protection can be achieved.

1. Introduction

Mg alloys possess the advantage of low specific weight, which has been responsible for its extensive use for casting parts. In addition, these alloys have other interesting properties for industrial use as structural components such as high thermal conductivity, damping properties, dimensional stability and recyclability. Regarding the aerospace industry, they might have an important technological impact for manufacturing low weight structures, resulting in significant fuel saving and decreased CO_2 emissions [1–3]. Nevertheless, Mg alloys are extremely susceptible to corrosion damage and this is a troublesome issue faced by the industry.

Corrosion can be delayed by the use of corrosion inhibitors, application of protective coatings (organic, inorganic or hybrid) or by the addition of alloying elements to produce more corrosion-resistant alloys. Merging the beneficial properties of both organic and inorganic compounds to design novel functional corrosion protective coatings is a challenge for industrial application. To be effective, these hybrid materials must present several characteristics, such as stable interactions with the metallic surface for good adhesion, homogeneity, low cost, and, according to the growing concerns of environmental protection, must be harmless to environment and to human beings. The sol–gel process has been considered one of the simplest routes to create such functional materials [4,5]. In a hybrid coating, the inorganic phase is responsible for increasing the bond strength between the substrate and the coating, hindering the action of aggressive species towards the substrate. On the other hand, the organic phase decreases the coating porosity and heterogeneity, and increases its thickness [6,7]. Hybrid coatings can be used either as pretreatments or as precursors of polymerization reactions with epoxy groups, providing a thick coating linked to the metallic substrate by covalent bonds [8].

GPTMS-TEOS based hybrid coatings have been used to protect Al and Al alloys [9–15], magnesium AZ31 alloys [16], and carbon steel [17]. All the authors have reported important improvement of the corrosion resistance of the coated metals and alloys. For instance, Rahimi et al. [9] employed a statistical design of experiment with multifactor analysis of variance to optimize the process parameters of the sol–gel coating wherein the corrosion current density was used as response [9]. It was observed that the corrosion resistance increased with the application of up to three sol–gel layers, while the wear resistance remained practically unchanged. The authors concluded that by proper choice of parameters, adherent, dense and protective hybrid coatings could be obtained [9,12]. However, it has been verified that in some cases corrosion appears after relatively short immersion times [17].

* Corresponding author.

http://dx.doi.org/10.1016/j.surfcoat.2015.12.049
0257-8972/

One of the strategies frequently used to improve the protective properties of hybrid coatings is their modification by the introduction of different nanoparticles and/or corrosion inhibitors. It has been reported that films with higher thicknesses, improved mechanical properties [18] as well as better anticorrosion resistance can be produced [18,19]. Zaharescu *et al.* [19] described the corrosion protection of Al and Mg alloys with SiO_2-methacrylate coatings doped with TiO_2–CeO_2 nanoparticles in chloride solution. They showed an improvement of the barrier properties as well as some signals of self-healing effect [19]. Superior corrosion resistance was also reported for a MTES(methyltriethoxysilane)-TEOS hybrid coating modified with SiO_2 or Ce and applied on a mild steel substrate [20].

Two critical issues that can effectively affect the anticorrosion behavior of nanoparticles loaded films are their dispersion within the film and the amount of added nanoparticles. Khelifa *et al.* [21] and Suegama *et al.* [22] claim that when the nanoparticles are uniformly dispersed within the film structure they can play a major role in the corrosion protection. In this sense Del Angel-Lopez *et al.* [23] demonstrate that the dispersion of ZrO_2:SiO_2 nanoparticles into polyurethane coatings by sonication and applied on carbon steel, led to systems with higher mechanical and corrosion resistance in chloride solution when compared to the coatings prepared by mechanical stirring [23]. Concerning the amount of nanoparticles, Santana *et al.* [24] investigated the anticorrosion performance of mono or bilayer TEOS-GPTMS hybrid coatings for the protection of carbon steel and reported the best results for the systems loaded with the highest amount of silica nanoparticles. On the other hand, Suegama *et al.* [25] indicate that an optimum amount of silica nanoparticles must be added to a hybrid coating for maximal corrosion protection of carbon steel in NaCl solution (300 mg l^{-1} in their case), a point of view shared by other authors [26–28]. It has been frequently reported that an excess of nanoparticles can introduce defects in the hybrid film structure, which become preferential pathways for electrolyte penetration.

As shown in the previous paragraphs, the literature survey indicates that the addition of nanoparticles to a hybrid coating increases it hardness [25] and thickness [24] and that improved barrier properties can be achieved when an optimum amount of nanoparticles is added to the hydrolysis solution. However, only few works address this strategy for the protection of Mg AZ31 parts, and only one concentration of SiO_2-metacrilate powder in the TiO_2:CeO_2 system was studied [19]. Thus, in the present work, the effect of the addition of different amounts (0 to 600 mg l^{-1}) of SiO_2 nanoparticles to a TEOS/GPTMS hybrid coating for the corrosion protection of AZ31 Mg alloy was evaluated by electrochemical measurements and their microstructure evaluated by SEM-EDS characterization.

2. Experimental procedure

2.1. Preparation of the Mg AZ31 substrate

AZ31 Mg alloy samples (dimensions 2 cm × 2 cm × 0.2 cm) were employed as substrate. Prior to coating application, the samples surfaces were successively wet-grinded down to 1200 using silicon carbide sandpaper. After the grinding procedure, the substrate was thoroughly cleaned with distilled water, rinsed with ethanol in an ultrasonic bath, gently wiped with filter paper and stored in a desiccator.

2.2. Coating methodology

The coating was prepared as following: 7.0 ml solution of tetraethyl orthosilane (TEOS) with 5.0 ml of (3-glycidoxypropyl)trimethoxysilane (GPTMS) were blended together with 12 ml of 70/30% v/v ethanol/water solution, pH 1.5 (nitric acid) at 25 °C. Seven distinct concentrations (0, 25, 50, 100, 300, 400 and 600 mg l^{-1}) of SiO_2 nanoparticles (CAB-O-SIL® TS-6) were added to the mixture, and then the solution was homogenized for one hour at room temperature. Therefore, the hydrolysis of the hybrid coating was performed in the presence of SiO_2 nanoparticles. Then, the AZ31 Mg alloy samples were dipped into the precursor solution at 8 cm min^{-1}, remaining there for 2 min; afterwards they were withdrawn at the same rate and subjected to a curing procedure at 50 °C for 24 h.

Preliminary tests were performed with different numbers of layers of the GPTMS-TEOS film doped with 100 mg l^{-1} of SiO_2. It was verified that when 3 or 5 layers of the hybrid coating were applied under the conditions described above, the resultant coatings showed stress and the impedance values were lower than those obtained when only one layer was applied. Therefore, all coatings described in this work are single layer.

2.3. Techniques

The corrosion resistance of the coated and uncoated Mg samples was evaluated in a classic three-electrode electrochemical cell by means of E_{OC} and EIS measurements carried out in naturally aerated and unstirred 0.1 mol l^{-1} NaCl electrolyte at 25 °C. The volume of electrolyte was 80 ml. The coated samples were used as working electrode, an Ag/AgCl/KCl(3 mol l^{-1}) electrode, connected to the electrolytic solution through a Luggin capillary, was used as reference, and a Pt network as counter electrode. The area of the working electrode exposed to the aggressive electrolyte was 1.0 cm^2. E_{OC} versus time and EIS measurements were carried out using a potenciostat–galvanostat AUTOLAB, PGSTAT302N model equipped with an impedance modulus. The EIS measurements were acquired for immersion times up to 48 h, and the impedance diagrams were performed by applying a 10 mV (rms) sinusoidal perturbation, from 5×10^4 to 1×10^{-2} Hz recording 10 points per frequency decade. The measurements were performed in triplicate. The first impedance diagram was acquired after 1 h immersion in the testing electrolyte, after E_{OC} stabilization. For quantitative analysis, the EIS results for the coated systems that presented the best anticorrosion performance were fitted by means of equivalent electric circuits (EEC) using the Z-view® software. All experimental data were tested for consistency with the Kramers–Kronig transform, and only those points passing the test are presented and discussed in the paper.

The changes of the samples surfaces with immersion time were accompanied by taking photos in situ at a rate of 1 photo/h in 0.1 mol l^{-1} NaCl solution using an electrochemical cell previously described [29].

The morphological characteristics of the uncoated and coated samples were examined by field emission scanning electron microscopy (FE-SEM JEOL, model JSM-7500F), whereas the bare surface was observed by SEM before and after EIS measurements. EDS (Thermo Scientific) coupled to the SEM system was used for chemical composition analysis.

The coatings thicknesses were estimated from the analysis of cross-sectional images. Only samples without and with 300 and 400 mg l^{-1} of SiO_2 were examined.

3. Results and discussion

3.1. Substrate and coatings characterization

SEM surface images of the uncoated AZ31 alloy before and after 48 h immersion in chloride solution are shown in Figs. 1(A) and 2(A), respectively. Before immersion, the bare substrate shows the marks of surface preparation. After the corrosion test, those marks are still present and no continuous corrosion product layer can be detected on the sample surface, but scattered corrosion products could be seen.

The top views of the as-prepared coatings show homogeneous and crack-free films, being all marks originated from the surface preparation covered by the hybrid material (Figs. 1(B-D)). At low magnifications, the film without nanoparticles shows defects (Fig. 1(B)), which are not noticed when 300 or 400 mg l^{-1} SiO_2 nanoparticles were added (Fig. 1(C) and (D)). Agglomeration of SiO_2 nanoparticles was not

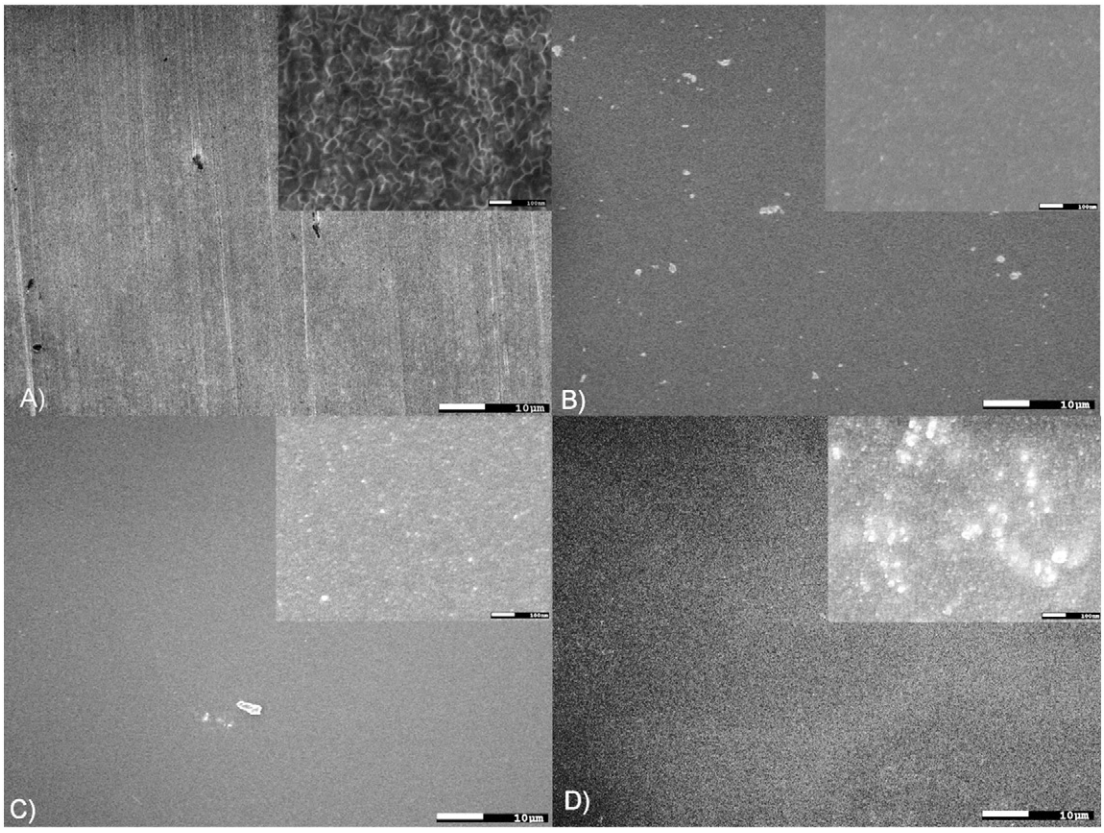

Fig. 1. SEM micrographs of the AZ31 alloy before immersion: bare (A), and coated with the hybrid without SiO_2 nanopartciles (B), with 300 mg l^{-1} SiO_2 (C) and with 400 mg l^{-1} SiO_2 (D). Inset: FE-SEM micrographs for 100,000× of magnification.

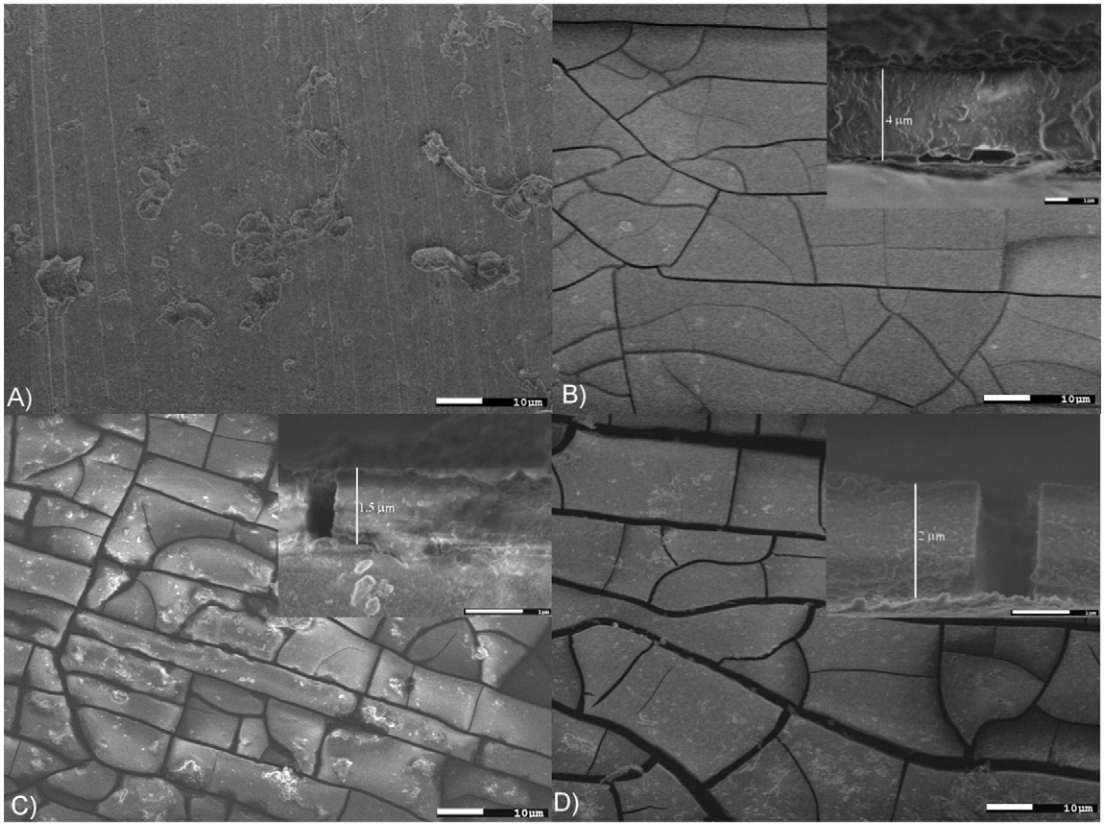

Fig. 2. SEM micrographs of the AZ31 alloy: bare(A), and coated with the hybrid without SiO_2 nanoparticles (B), with 300 mg l^{-1} SiO_2 (C) and with 400 mg l^{-1} SiO_2 (D) after 48 h of immersion in 0.1 mol l^{-1} NaCl solution. Inset: FE-SEM cross-section micrographs.

observed at low magnifications, however, clusters of particles inside and outside the hybrid film can be noticed at high magnifications (insert of Fig. 1(C) and (D)), which is in accordance with previously published results who reported clustering of nanoparticles in modified silane [30,31] and hybrid [20] films. The coating doped with 300 mg l^{-1} SiO_2 depicts only submicron agglomerates, while the film doped with 400 mg l^{-1} SiO_2 shows great amount of bigger agglomerates. When the particles concentration was increased to 600 mg l^{-1} SiO_2, defects and cracks were observed on the film surface, probably due to the stress produced inside it. This suggests that the dopant will offer no protection benefit compared to the non-doped coating. Suegama *et al.* [22] and Zandi Zand *et al.* [31] verified that the addition of an excess of nanoparticles to silane [22] and hybrid [31] films hinder the anticorrosion properties of the films, which was associated to the introduction of defective sites [31]. In accordance with our results, these latter authors [31] also verified the presence of defects in the unmodified hybrid films and that defect free coatings were produced when an intermediate amount of CeO_2 nanoparticles was added to the hybrid formulation.

After 48 h immersion, all coated samples show the well-known cracked-mud morphology (Fig. 2(B-D)), common when stable corrosion products are formed on Mg [32], which extends throughout the entire surface, as shown in the cross-section images (insert in Fig. 2). This suggests that such coatings may act essentially as adhesion promoters and short-term corrosion protectors. SEM cross-section images of as-prepared samples (Figs. 3(A) and (B)) allowed estimating the coating thickness to be around 3, without, and 4 μm, with different amounts of SiO_2 nanoparticles, showing that nanoparticles incorporation increased the coating thickness, as previously observed for similar systems [25].

3.2. Open circuit potential

The E_{OC} measured after 1, 7, 24, 30 and 48 h immersion in the 0.1 mol l^{-1} NaCl electrolyte are depicted in Table 1. For short immersion times, the E_{OC} for some of the coatings shift towards more negative values in comparison with the uncoated sample, suggesting higher electrochemical activity, however, as time elapses, all the measurements converge, showing the predominance of the substrate response, which can be likely ascribed to electrolyte penetration through the coatings and to the formation of corrosion products.

3.3. Electrochemical impedance spectroscopy (EIS)

The impedance plots for the bare AZ31 substrate in the 0.1 mol l^{-1} NaCl electrolyte are displayed in Fig. 4. The diagrams show an increase of the capacitive loop diameter as immersion time elapses (Fig. 4(A)). The associated phase angle diagrams (Fig. 4(B)) present a broad time constant in the medium frequency region (≈30 Hz), which maximum

Table 1
E_{OC} values after 1, 7, 24, 30 and 48 h of immersion in 0.1 mol l^{-1} NaCl solution for AZ31 Mg alloy with and without hybrid coatings modified with different amounts of SiO_2 nanoparticles.

Sample	E_{OC}/($V_{/Ag\|AgCl\|KCl\ 3\ mol\ l^{-1}}$)				
Time	1 h	7 h	24 h	30 h	48 h
Substrate	−1.40	−1.42	−1.30	−1.33	−1.26
0 SiO_2 mg l^{-1}	−1.38	−1.45	−1.24	−1.19	−1.25
25 SiO_2 mg l^{-1}	−1.43	−1.35	−1.22	−1.20	−1.26
50 SiO_2 mg l^{-1}	−1.51	−1.37	−1.32	−1.28	−1.25
100 SiO_2 mg l^{-1}	−1.49	−1.48	−1.30	−1.33	−1.25
300 SiO_2 mg l^{-1}	−1.36	−1.32	−1.29	−1.37	−1.33
400 SiO_2 mg l^{-1}	−1.49	−1.44	−1.32	−1.30	−1.28
600 SiO_2 mg l^{-1}	−1.44	−1.39	−1.30	−1.25	−1.27

slightly shifts to lower frequency values. This response indicates a decrease in the kinetics of the interfacial process and is commonly observed in bare Mg alloys exposed to neutral aggressive electrolytes. Indeed, magnesium corrosion is accompanied by strong surface alkalinization due to the formation of hydroxyl ions because of the cathodic reaction. This process leads to the precipitation of $Mg(OH)_2$, and the surface is covered by a porous corrosion product layer [3,32–34] that may induce a slight increase on the impedance of the system [32]. Observing the alloy surface immersed in the test electrolyte at selected times support the proposed mechanism. The presence of hydrogen bubbles originated from the H^+ reduction reaction, and the formation of dispersed corrosion products were evident. After 48 h immersion, some bright regions could be observed on the sample surface, pointing to the detachment of the corrosion product layer, which seems to be loosely adhered to the electrode.

An EEC with an R_s in series with a R_i//Q_i sub-circuit (Fig. 5) was used to fit the EIS data depicted in Fig. 4. In the proposed model, R_s corresponds to the electrolyte resistance, R_i refers to the charge transfer resistance and the constant phase element, Q_i, to the electrical double layer capacitance. In the circuit, the capacity was substituted for a Q in order to take into account the non-ideality of the system. The Q element is constituted by the admittance Y and the exponent "*n*". When $n = 1$ the electrode behaves ideally and Q becomes a pure capacitor. On the other hand, $n = 0.5$ suggests a diffusion-controlled process or a porous material [35–37], and when $0.5 < n < 1$ the deviation from the ideal behavior is associated to a heterogeneous, rough electrode or to non-homogeneous current distribution on the electrode surface [38–41], or either to a non-homogeneous distribution of the electrical properties within the oxide film or coating [42].

For the uncoated sample, EIS data below 1 Hz did not pass the KKT test indicating that the system is no longer stable. H_2 evolution is the main cathodic reaction for Mg immersed in neutral aerated medium [43]. As previously stated, H_2 bubbles were seen to evolve from the

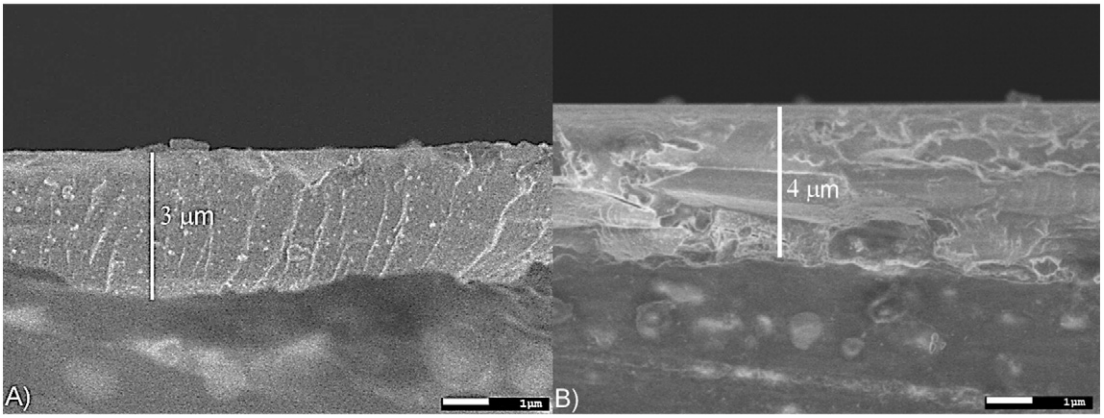

Fig. 3. SEM cross-section images of the AZ31 alloy coated with hybrid without SiO_2 nanoparticles (A), with 400 mg l^{-1} SiO_2 (B).

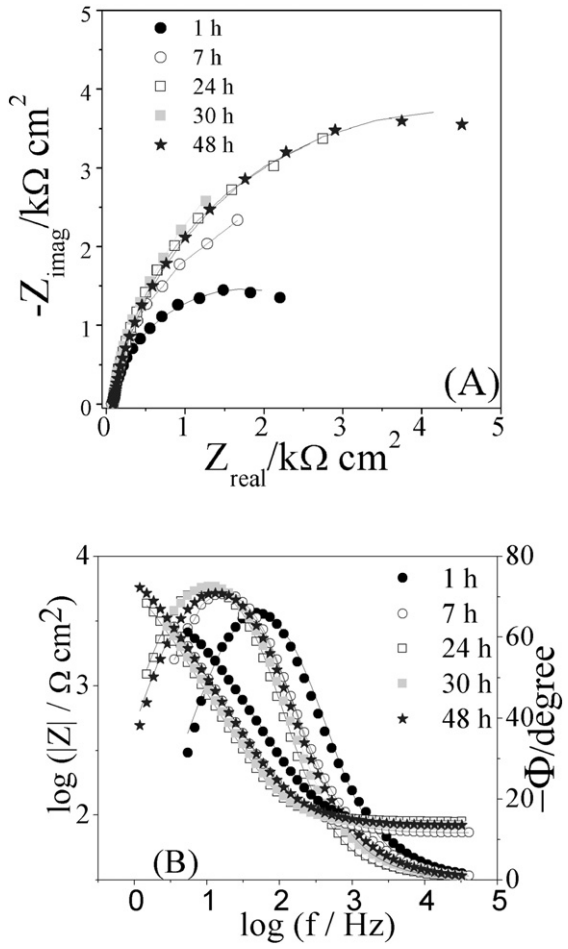

Fig. 4. Experimental (symbols) and fitted (solid lines) EIS diagrams for the AZ31 Mg alloy in 0.1 mol l^{-1} NaCl solution recorded at different immersion times. (A) Nyquist and (B) Bode plots.

sample surface. Therefore, it is likely that the presence of such molecules on the sample surface before their evolution would provoke potential oscillation, impeding the acquisition of reliable low frequency EIS data.

Table 2 depicts the results of the fitting procedure for the bare substrate with the EEC of Fig. 5. It shows that R_i values initially increases (from 1 to 24 h) and them presents a relatively stable response. On the other hand, Q_i shows an almost capacitive response, with "*n*" close to unity, remaining relatively constant.

In order to compare the different capacitive responses and to better explain the EIS behavior of the bare sample, the effective capacitances, $C_{eff\ i}$, were calculated from the coefficients Q of the constant phase elements and the *n* exponents using Eq. (1) [24,44]:

$$C_{eff} = \frac{(QR)^{1/n}}{R}. \quad (1)$$

The calculated values were added to Tables 2-6. Table 2 shows that from 7 h immersion $C_{eff\ i}$ values lie slightly below those normally ascribed to the double layer capacity (C_{dl} = 50 μF cm^{-2} [32]). On the other hand, for 1 h immersion, $C_{eff\ i}$ (7 μF cm^{-2}) lies well below this

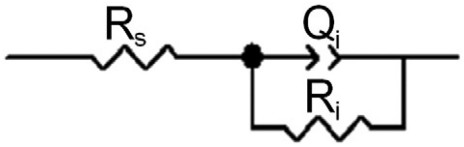

Fig. 5. Equivalent electrical circuit used to fit the EIS diagrams of Fig. 4.

Table 2
EEC parameters, relative errors percentage, and the variance of the residual error (χ^2) obtained for the AZ31 alloy in 0.1 mol l^{-1} NaCl solution for different immersion times.

Time/h	1	7	24	30	48
R_s/Ω cm^2	78 (0.7)	76 (0.7)	91 (0.3)	84 (0.4)	86 (0.6)
R_i/kΩ cm^2	3.4 (2.5)	6.7 (5.7)	8.0 (1.8)	10 (4.0)	8.6 (2.4)
Y_i/μF cm^{-2} s$^{(ni-1)}$	10 (2.8)	20 (2.7)	24 (0.9)	24 (1.3)	20 (1.6)
$C_{eff\ i}$/μF cm^{-2}	7.2	16	21	21	17
n_i	0.91 (0.5)	0.91 (0.5)	0.93 (0.2)	0.91 (0.3)	0.91 (0.4)
$\chi^2/10^{-3}$	3.7	6.3	1.3	1.8	3.7

value. Baril and Pebere [32], investigating the corrosion behavior of pure Mg in sodium sulfate solution, found similar capacity values for the high frequency loop, which was ascribed to both charge transfer and a film effect. Literature indicates that Mg develops a thin, dense, amorphous, and relatively dehydrated film when exposed to air [45],which may assume a duplex structure (a MgO layer in contact with the substrate and a top porous MgO/$Mg(OH)_2$ layer) when exposed to chloride solutions [46]. Therefore, it is proposed that the initial active (low resistance) behavior could be ascribed to a fast dissolution of the more active surface layer together with the hydration and partial dissolution of the air-formed oxide film upon exposure to the aggressive electrolyte. Conversely, for longer immersion times, the corrosion process would occur in an electrode surface covered by a very thin porous oxide layer [46], explaining why $C_{eff\ i}$ values increase and become only slightly lower than that normally ascribed to C_{dl}. This interpretation holds also for the samples covered with the hybrid layer (Tables 3-6), and, therefore, variation of the $C_{eff\ i}$ will no longer be commented.

Fig. 6 shows the EIS responses of all studied samples after 1 h of immersion. The coated samples presented Z_{real} values higher than the bare substrate indicating improvement of the AZ31 Mg alloy corrosion resistance. Among them, the sample protected with the hybrid modified with 100 mg l^{-1} SiO_2 displays the highest impedance modulus that, at the lowest frequency point, is about 400 kΩ cm^2, being more than two orders of magnitude higher than that estimated for the bare substrate from the EEC fitting (≈3.4 kΩ cm^2 — Table 2). A good response was also detected for the unmodified coating (0 mg l^{-1}), with low frequency (LF) impedance of about 150 kΩ cm^2. A particularly unstable behavior was found for the system with 300 mg l^{-1} SiO_2. It exhibited low frequency data scattering and only few experimental points passed the KKT test. This trend was verified for three different assays and indicates faster electrolyte uptake with early onset of the corrosion process. It is likely that hydrogen gas entrapment at the coating-substrate interface would cause coating blistering and consequent potential fluctuations

Table 3
EEC parameters, relative errors percentage, and the variance of the residual error (χ^2) obtained in 0.1 mol l^{-1} NaCl solution for the AZ31 alloy protected with the hybrid coating without SiO_2 nanoparticles.

Time/h	1	7	24	30	48
R_s/Ω cm^2	290 (31)	86 (2.5)	46 (8.2)	47 (7.3)	74 (0.3)
R_{coat}/kΩ cm^2	0.6 (1.4)				
Y_{coat}/μF cm^{-2} s$^{(n-1)}$	0.3 (12)				
n	0.68 (1.4)				
Y_{oxide}/μF cm^{-2} s$^{(n_{oxide}-1)}$	1.9 (28)	6.1 (8.6)	6.5 (14)	6.0 (8.9)	5.2 (17)
$C_{eff\ oxide}$/μF cm^{-2}	1.0				5.2
n_{oxide}	0.91 (3.7)	0.75 (6.0)	0.5 (8.5)	0.5 (8.6)	1.0 (1.7)
R_{oxide}/kΩ cm^2	1.1 (20)	0.01 (18)	0.04 (9.5)	0.04 (8.5)	0.05 (17)
Y_i/μF cm^{-2} s$^{(ni-1)}$	2.6 (22)	4.1 (9.4)	21 (2.0)	18 (1.5)	9.6 (10)
$C_{eff\ i}$/μF cm^{-2}	2.4	4.0	20	17	7.3
n_i	0.80 (1.4)	0.99 (1.0)	0.95 (0.3)	0.95 (0.3)	0.86 (0.5)
R_i/kΩ cm^2	281 (1.5)	19 (1.0)	14 (1.1)	26 (1.0)	20 (0.5)
$\chi^2/10^{-3}$	0.3	2.4	1.0	0.9	0.4

Table 4
EEC parameters, relative errors percentage, and the variance of the residual error (χ^2) obtained in 0.1 mol l^{-1} NaCl solution for the AZ31 alloy protected with the hybrid coating with 25 mg l^{-1} SiO_2 nanoparticles.

Time/h	1	7	24	30	48
R_s/Ω cm^2	260 (2.6)	56 (6.6)	55 (4.8)	46 (6.8)	78 (0.2)
R_{coat}/kΩ cm^2	0.5 (1.3)				
Y_{coat}/μF cm^{-2} $s^{(n-1)}$	0.3 (16)				
n	0.67 (2.0)				
Y_{oxide}/μF cm^{-2} $s^{(n_{oxide}-1)}$	5.1 (19)	6.1 (19)	7.7 (13)	6.1 (13)	18 (1.3)
$C_{eff\ oxide}$/μF cm^{-2}	2.0				11
n_{oxide}	0.83 (2.8)	0.5 (11)	0.5 (11)	0.5 (11)	0.92 (0.2)
R_{oxide}/kΩ cm^2	1.8 (23)	0.03 (11)	0.03 (1.6)	0.04 (9.0)	0.2 (18)
Y_i/μF cm^{-2} $s(n_i-1)$	3.1 (30)	13 (2.6)	30 (1.6)	27 (1.5)	2.3 (8.9)
$C_{eff\ i}$/μF cm^{-2}	2.4	11	29	26	2.3
n_i	0.87 (4.2)	0.94 (0.4)	0.95 (0.3)	0.95 (0.3)	1.0 (5.4)
R_i/kΩ cm^2	62 (0.9)	6.6 (1.5)	14 (1.1)	18 (1.1)	17 (0.4)
$\chi^2/10^{-3}$	0.5	0.6	0.8	0.8	0.5

and LF data scattering. Photos of this sample surface taken at 0, 24 and 72 h immersion in the test electrolyte showing the presence of pockets underneath the coating (Fig. 7) support this hypothesis.

As shown in the insert of Fig. 6(A), the Nyquist plots (and the phase angle evolution) for the coated samples exhibit a small high frequency capacitive loop, which, as will be shown in the subsequent Figs., vanishes for longer immersion periods.

Fig. 8 presents the impedance diagrams for the AZ31 Mg alloy protected with the hybrid coating without SiO_2 nanoparticles (blank coating) in 0.1 mol l^{-1} NaCl electrolyte for test periods longer than 7 h. The Nyquist plots (Fig. 8(A)) are composed by only one well-defined and depressed capacitive loop which modulus is considerably smaller than that observed after 1 h immersion (Fig. 6(B)). For longer test periods, an oscillating impedance response was observed, indicating the precipitation of non-protective corrosion products. Contrarily to the spectra taken after 1 h (Fig. 6(B)), the phase angle plots (Fig. 8(B)) clearly show only a single broad time constant in the whole frequency domain, which origin will be discussed in the EEC fitting procedure. Identical samples immersed in the test electrolyte showed the buildup of corrosion products with immersion time, but less gas was evolved in comparison to the bare substrate and, at the end of the

Table 5
EEC parameters, relative errors percentage, and the variance of the residual error (χ^2) obtained in 0.1 mol l^{-1} NaCl solution for the AZ31 alloy protected with the hybrid coating with 100 mg l^{-1} SiO_2 nanoparticles.

Time/h	1	7	24	30	48
R_s/Ω cm^2	310 (4.6)	102 (1.0)	90 (0.4)	69 (0.2)	66 (0.4)
R_{coat}/kΩ cm^2	0.9 (2.8)				
Y_{coat}/μF cm^{-2} $s^{(n-1)}$	0.1 (15)				
n	0.75 (2.1)				
Y_{oxide}/μF cm^{-2} $s^{(n_{oxide}-1)}$	1.4 (19)	7.7 (2.3)	19 (4.3)	7.0 (10)	12 (3.4)
$C_{eff\ oxide}$/μF cm^{-2}	0.09	0.05	7.9	7.0	9.5
n_{oxide}	0.94 (2.6)	0.78 (2.3)	0.90 (0.8)	1.0 (1.2)	0.96 (0.3)
R_{oxide}/kΩ cm^2	1.3 (10)	0.009 (18)	0.02 (16)	0.04 (9.4)	0.3 (19)
Y_i/μF cm^{-2} $s^{(ni-1)}$	3.4 (8.3)	4.0 (5.4)	8.0 (11)	17 (4.8)	3.2 (9.5)
$C_{eff\ i}$/μF cm^{-2}	4.0	4.0	8.0	15	2.8
n_i	0.79 (0.3)	1.0 (5.0)	1.0 (5.5)	0.85 (8.0)	0.95 (7.5)
R_i/kΩ cm^2	547 (1.0)	14 (1.1)	19 (0.6)	28 (0.6)	18 (1.4)
$\chi^2/10^{-3}$	0.3	1.4	0.6	0.5	1.5

Table 6
EEC parameters, relative errors percentage, and the variance of the residual error (χ^2) obtained in 0.1 mol l^{-1} NaCl solution for the AZ31 alloy protected with the hybrid coating with 300 mg l^{-1} SiO_2 nanoparticles.

Time/h	7	24	30	48
R_s/Ω cm^2	101 (0.5)	64 (0.9)	76 (0.6)	82 (0.5)
R_{coat}/kΩ cm^2	48 (2.8)			
Y_{coat}/μF cm^{-2} $s^{(n-1)}$	11 (2.3)			
$C_{eff\ coat}$/μF cm^{-2}	10			
n	0.89 (0.1)			
Y_{oxide}/μF cm^{-2} $s^{(n_{oxide}-1)}$	30 (8.2)	19 (7.0)	22 (4.0)	13 (6.2)
$C_{eff\ oxide}$/μF cm^{-2}		2.7	8.2	10
n_{oxide}	0.64 (1.4)	0.80 (2.2)	0.87 (0.6)	0.97 (10)
R_{ox}/kΩ cm^2	0.2 (4.2)	0.02 (9.8)	0.06 (17)	0.06 (8.0)
Y_i/μF cm^{-2} $s^{(ni-1)}$	39 (18)	8.5 (12)	3.9 (10)	10 (9.5)
$C_{eff\ i}$/μF cm^{-2}	39	8.5	3.9	9.1
n_i	1.0 (5.6)	1.0 (1.4)	1.0 (7.9)	0.95 (10)
R_i/kΩ cm^2	55 (7.0)	30 (1.2)	35 (1.0)	15 (1.9)
$\chi^2/10^{-3}$	0.1	3.9	2.1	2.0

immersion period, no bright region was seen on the sample surface, indicating that the corrosion product layer remains adherent to the substrate.

The EIS response of the AZ31 Mg alloy protected with the unmodified coating was fitted using the EECs of Fig. 9. In the EEC of Fig. 9(A), used only to fit the results for 1 h immersion, [R_{coat}//Q_{coat}] was ascribed to the coating response, [R_{oxide}//Q_{oxide}] was associated with the properties of the magnesium oxide layer (oxides and hydroxides underneath

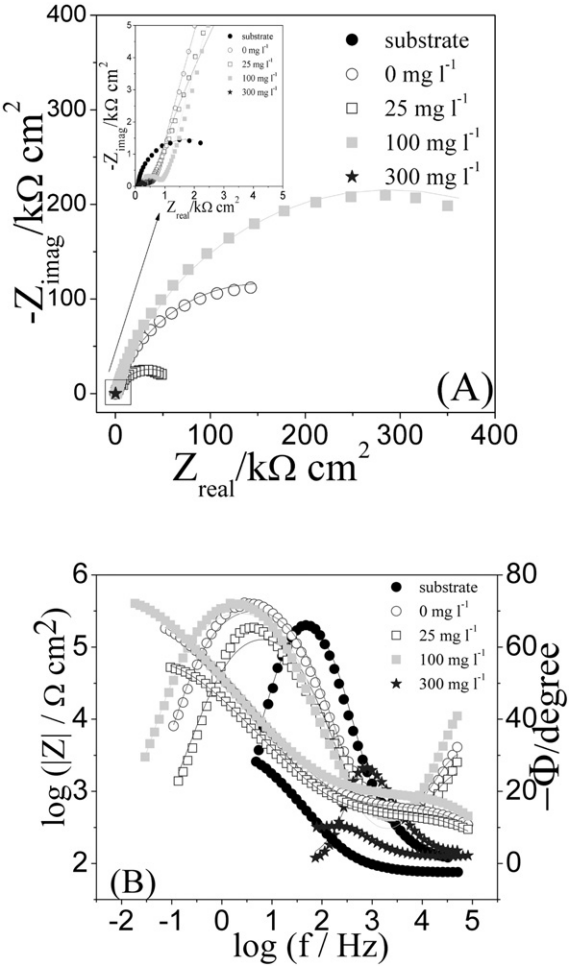

Fig. 6. Experimental EIS diagrams in 0.1 mol l^{-1} NaCl solution recorded at 1 h immersion time for the AZ31 Mg alloy, protected with hybrid coating with or without SiO_2 nanoparticles. (A) Nyquist and (B) Bode plots.

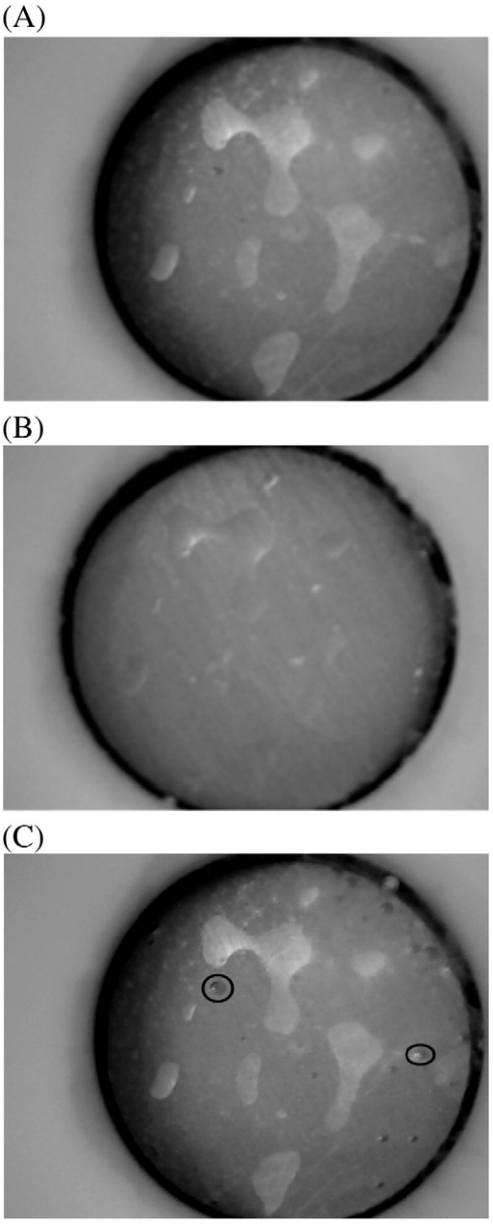

Fig. 7. Photos of the AZ31 Mg alloy protected with the hybrid coating with the addition of 300 mg l^{-1} SiO_2. Images taken after (A) 0, (B) 24, and (C) 72 h of immersion in 0.1 mol l^{-1} NaCl solution. Exposed area = 1 cm^2.

the coating), whereas the [R_i//Q_i] sub-circuit was assigned to interfacial processes: electrical double layer charging and charge transfer resistance [47], as for the bare sample. The EEC of Fig. 9(B) is a simplification of the previous one where the coating and the oxide responses were merged; therefore, R_{oxide}//Q_{oxide} represents the mixed response of the hybrid coating and the corrosion product layer. The fitted values are presented in Table 3. It must be emphasized that, for immersion times longer than 7 h, attempts to fit the diagrams with only one time constant were unfruitful and a two time constant EEC had to be employed, this was also verified for the other coated samples.

For the shortest immersion time (1 h), even though the coating is relatively thick, R_{coat} is small (about 600 Ω cm^2), indicating that it does not effectively hinder electrolyte access to the metallic surface, R_{oxide} was about 1 kΩ cm^2, also pointing to weak protection ability of the corrosion product layer. For 7 h and longer periods, R_{oxide} dramatically falls, indicating that the barrier properties of the coating and of the subsequently formed corrosion product layer are rather poor, and low resistance is offered to electrolyte penetration inside the pores.

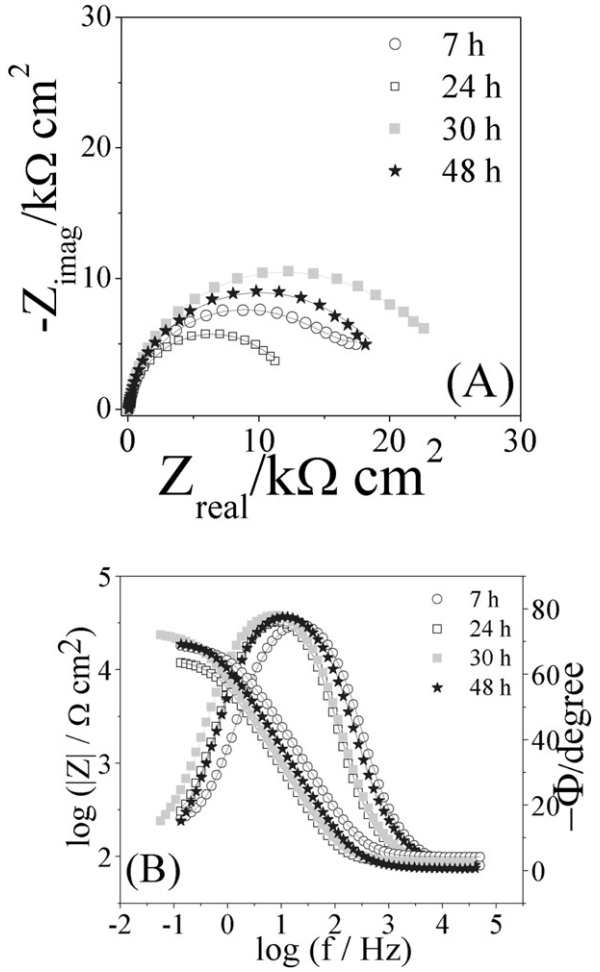

Fig. 8. Experimental (symbols) and fitted (solid lines) EIS diagrams in 0.1 mol l^{-1} NaCl solution for the AZ31 Mg alloy protected with the hybrid coating without SiO_2 nanoparticles. (A) Nyquist and (B) Bode plots.

On the other hand, the coefficient of Q_{oxide} (Y), which depends on the properties of the oxide layer, increases from 1 to 7 h and then remains approximately constant. This tendency together with the electrode surface observation suggest that, for the shortest immersion period, where the corrosion product buildup is low, the response of the hybrid layer must predominate. On the other hand, for immersion times longer than 7 h, the capacitive response of the porous corrosion product layer must prevail, indicating that electrolyte can easily penetrate the coating. This interpretation is supported by the low value of the "*n*" exponent (close to 0.5 for immersion times superior to 7 h), indicating that the

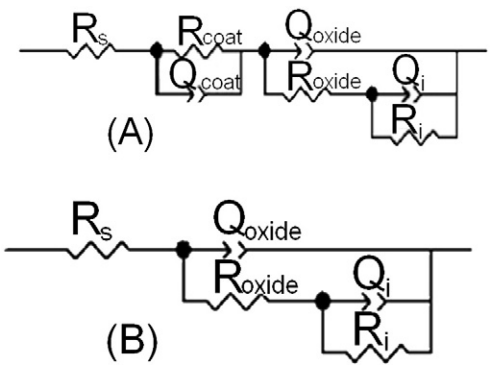

Fig. 9. EEC used to fit the EIS diagrams of coated samples: (A) for 1 h immersion, (B) for immersion times higher than 7 h.

ensemble "coating + corrosion product layer" behaves as a porous electrode [36,48,49]. However, at the end of the test period, 48 h, Y_{oxide} responds as a capacitor, indicating that the corrosion product layer becomes more compact and spreads all over the surface with uniform characteristics. The presence of such layer on the electrode surface is supported by the SEM images (Fig. 2(B–D)) showing the cracked mud structure of the Mg oxide/hydroxide layer on the coated samples.

For the fitting results where the Q exponents (n) were close to 1, C_{eff} values were determined from Eq. (1). For the coating it is around 5 nF cm^{-2}, which is an expected value for an hybrid layer with thickness between 3 and 5 μm, considering that the dielectric constant of this coating is typically between 3 and 8 [50]. For the oxide layer, C_{eff} is about 1 μF cm^{-2} and 5.2 μF cm^{-2} after 1 and 48 h immersion, respectively, indicating that the corrosion product layer, even though thick (cf. Fig. 2) does not offer a barrier to electrolyte penetration and is rather permeable to electrolyte and aggressive species penetration. For the intermediate immersion times, C_{eff} was not determined as "n" was close to 0.5 and a porous electrode response is obtained.

Concerning the time constant associated to the interfacial phenomena (Q_i and R_i), the values presented in Table 3 show that Y_i responds close to a capacitor ($n > 0.8$). The C_{eff} values for 1 h shows a charge transfer response mixed with a film effect [32] (see the discussion for the uncoated sample) and for times >1 h it increases and stabilizes around values expected for the double layer capacitance [51,52], still under the influence of a very thin porous oxide surface film [46]. On the other hand, R_i dramatically falls between 1 and 7 h, indicating that the electrolyte easily reached the bare metal, which is coherent with the low R_{oxide} values. For immersion times longer than 7 h, as for the bare samples, R_i presents an oscillating behavior with values about two times higher them those presented in Table 2 indicating that the presence of the coating slightly increases the corrosion resistance of the substrate.

The precipitation of corrosion products on the electrode surface, after some hours of immersion, is supported by the SEM images (Fig. 2(B)) and EDS analysis (Fig. 10), that did not detected magnesium prior to immersion (EDS spectrum of Fig. 10(A)), confirming that the coating is uniform and thick, and showed high amount of Mg after 48 h immersion in the test electrolyte (EDS spectrum and mapping of Fig. 10(B)).

The EIS diagrams after more than 7 h immersion in the test electrolyte for the sample protected with the hybrid coating modified with 25 mg l^{-1} SiO_2 nanoparticles are presented in Fig. 11 (note: the 1 h diagram is included in Fig. 6). Qualitatively the results were very similar to those observed for the sample protected with the unmodified coating. Initially, the impedance modulus greatly decreases from 1 to 7 h of test, indicating fast electrolyte uptake. In addition, the Nyquist plot taken after 1 h immersion is composed by a small capacitive loop at high frequencies followed by another broad capacitive loop, whereas for the remainder of the test period it is composed by a single depressed capacitive loop; and, except for the 1 h diagram, the Bode plots reveal only one broad time constant. In addition, the impedance moduli are of the same order of magnitude to those previously presented. However, instead of exhibiting an oscillating response with immersion time, after the initial fall, impedance increases from 7 to 48 h of immersion, indicating a gradual buildup of an interfacial layer with slightly better protective properties.

Table 4 displays the results of the fitting procedure of the diagrams of Fig. 11 with the EECs of Fig. 9. The effective capacitances (C_{eff}) determined for this sample were quite similar to those obtained for the unmodified coating, however $C_{eff\ oxide}$ is slightly higher, indicating that a thinner oxide layer is being built. The comparison of the resistance values presented in Table 4 with those of Table 3 indicates that the anticorrosion properties of the system is slightly hindered when 25 mg l^{-1} of silica nanoparticles were added to the hybrid formulation, as the low frequency resistance (R_i) is smaller for the modified coating. However, lower gas evolution and brighter surface were observed compared to the coating without SiO_2 addition. This indicates that, somehow, the addition of the silica nanoparticles to the hybrid formulation slows down the corrosive attack and/or the precipitation of the corrosion product layer. Baskaran *et al.* [53], using hydrotalcite, clearly demonstrated that Mg ions can form stable solid solution compounds with silicates. On the other hand, Palanivel *et al.* [54] verified that the addition of few mg l^{-1} of SiO_2 nanoparticles to a silane formulation increased the protection afforded to Al alloy 2024-T3. They proposed that the nanoparticles could suppress the cathodic process by reacting with the cathodically generated hydroxyl ions forming SiO_3^{2-} ions that would then react with the Al^{3+} cations formed at the anodic sites, passivating the electrode surface and obstructing the corrosive attack [54]. Taking into account our experimental findings and the literature results, it is suggested that the formation of a magnesium silicate passive layer would hinder the interfacial pH increase, delaying the precipitation of the thick corrosion product layer and rendering the surface of the electrode protected with the modified coating brighter. On the other hand, the slow and gradual precipitation of the corrosion product layer at the electrode surface would explain the increase in the impedance modulus from 7 h to the end of the immersion period. This hypothesis is supported by the cross-section images presented in Fig. 2(B)–(D) that clearly show that a thicker corrosion product layer is formed on the sample protected with the blank coating when compared to the SiO_2 modified ones.

The EIS behavior as well as the appearance of the sample protected with the coating modified with 50 mg l^{-1} SiO_2 was very similar to those observed for the one modified with 25 mg l^{-1} and, therefore, they will not be presented. Fig. 12 shows the EIS response of the electrode protected with the hybrid coating modified with 100 mg l^{-1} SiO_2. The overall impedance behavior was very similar to those presented by the other coated samples and will not be further commented. Conversely, the electrode surface remains brighter than for the samples discussed previously. It is hypothesized that the hybrid coating delays the corrosive attack keeping the corrosion product layer adhered to the surface and also that it slows down its thickening, thus maintaining the surface brightness for a longer time. To support this hypothesis, EDS mapping was performed on the surface of a sample protected with a hybrid coating prior and after 48 h immersion test, the results are presented in Fig. 10. It can be verified that after the coating procedure, Fig. 10(A), no Mg sign could be detected (insert spectrum). On the other hand, after the immersion test, Fig. 10(B), both Mg and Si signs were observed, (both in the spectrum and uniformly distributed in the maps) indicating the build up of a Mg oxide/hydroxide corrosion product layer underneath the hybrid coating. At variance with what was verified for the bare sample, the hybrid seems to act as a physical barrier, impeding the detachment of the corrosion products from the electrode surface and improving the corrosion behavior.

The results of the fitting procedure of the diagrams of Fig. 12 with the EECs of Fig. 9 are presented in Table 5. For this sample Q_{oxide} did not show the capacitive response typical of a porous electrode, which can be ascribed to the slow precipitation of a corrosion product layer underneath the hybrid coating. However, R_{oxide} is still low, demonstrating that the system develops conductive pathways for electrolyte uptake. Compared to the previously reported results (Tables 2 to 4), after the strong decrease between 1 and 7 h, the interfacial resistance (R_i) continuously increases up to 30 h, attaining the highest value at this immersion time. This could be a consequence of the gradual formation of the corrosion product layer. However, after 48 h the impedance decreases again, being slightly smaller than that observed for both the unmodified and the 25 mg l^{-1} SiO_2 modified hybrid coating. At this time, even though the surface remains bright, hydrogen bubbles evolution became stronger. This indicates the acceleration of the corrosion reaction, justifying the decrease of the impedance modulus.

For the sample coated with the hybrid modified with 300 mg l^{-1} SiO_2 the data obtained for t ≥ 7 h are shown in Figs. 13(A) (B). Up to 30 h the impedance modulus values were greater than those obtained

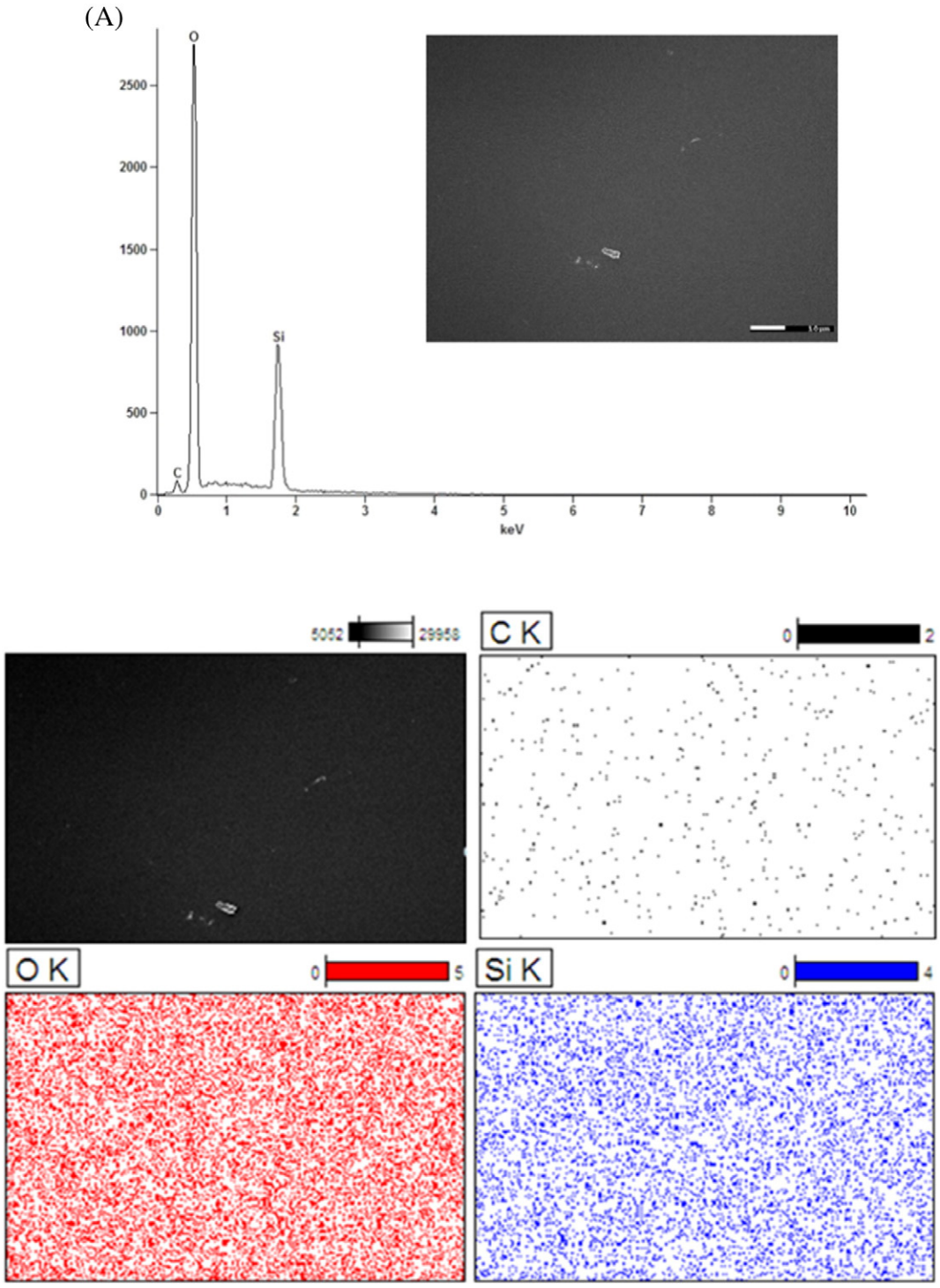

Fig. 10. EDS maps of C, O, Mg and Si elements recorded from an edge-on of the AZ31 alloy coated with the hybrid containing 300 mg l^{-1} SiO_2. (A) before immersion and (B) after 48 h of test in 0.1 mol l^{-1} NaCl solution.

for the previous samples, indicating increased anticorrosion properties. Regarding the Bode diagrams (Fig. 13(B)), the additional high frequency time constant was observed for the experiment performed at 7 h, whereas for the remainder of the immersion period the diagrams were similar to those obtained for the other samples.

As already stressed, for the samples coated with this formulation, the EIS diagrams acquired after 1 h immersion were characterized by a strong low frequency dispersion, therefore, they were not fitted with EEC. The EEC of Fig. 9(A) was employed to fit the diagram after 7 h of immersion, whereas the remainder of the data was fitted with the EEC of Fig. 9(B). The results are displayed in Table 6. The determined C_{eff} for the oxide layer was very similar to those found for the other samples coated with SiO_2 modified coatings, indicating comparable properties for the corrosion product layer. Besides being the only sample that exhibited a time constant directly\associated with the coating response after 7 h immersion, it presented the highest values of R_i up to 30 h of immersion, indicating superior efficacy in hindering the interfacial corrosion processes. However, after 48 h the low frequency data was scattered and the impedance greatly decreases, being the lowest among all the studied samples. This could be ascribed to wedging effects

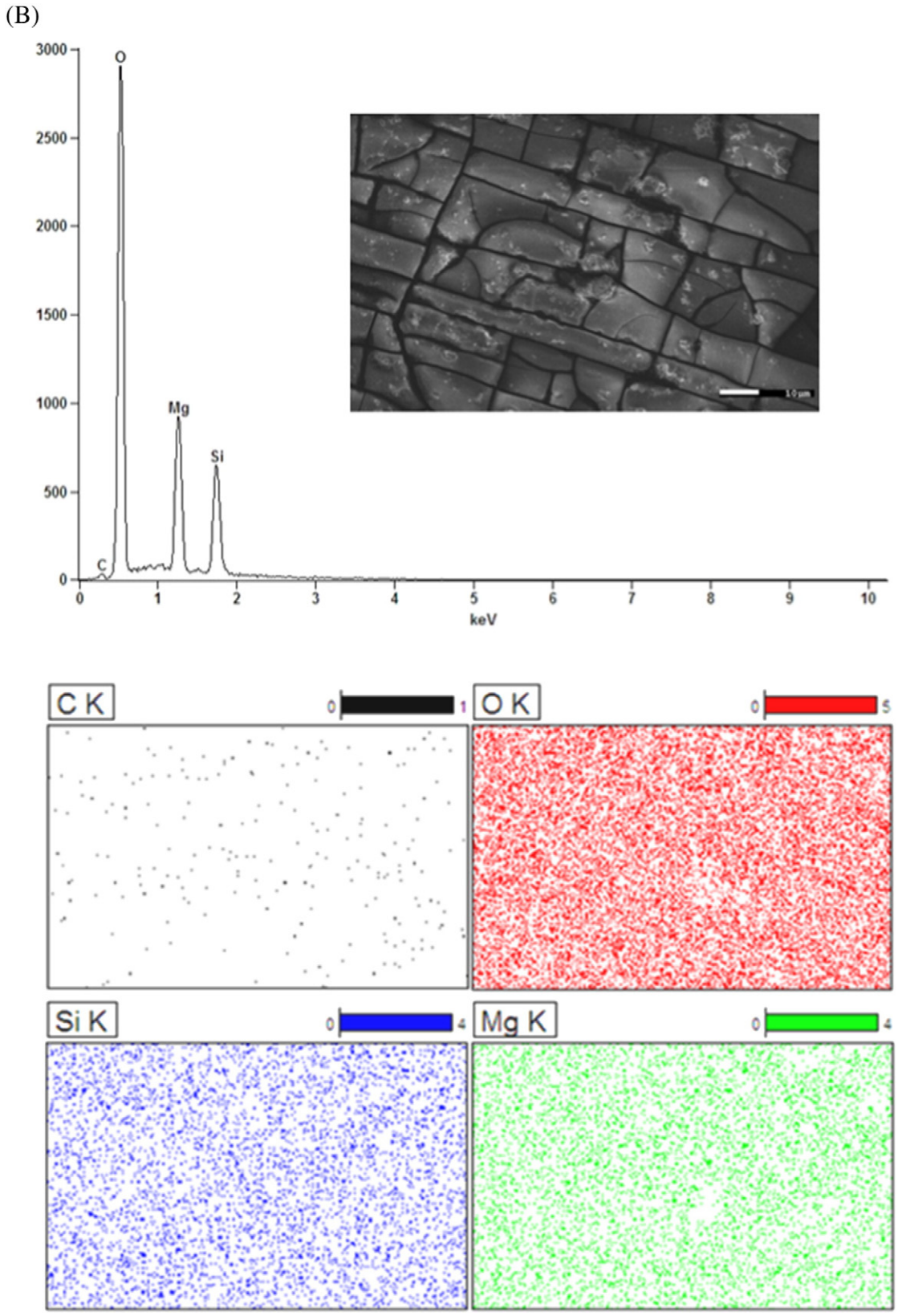

Fig. 10 (*continued*).

of corrosion products leading to local breakage of the coating, locally accelerating the corrosion process. Indeed, it was noticed that in some regions the coating was loosely adhered to the sample surface. In these regions, pockets were formed underneath the damaged coating (Fig. 7). The entrapment of hydrogen bubbles within these regions could explain the observed low frequency scattering of the EIS data.

Coatings prepared by adding 400 or 600 mg l^{-1} SiO_2 showed lower impedance than samples with 100 or 300 mg l^{-1} for all immersion

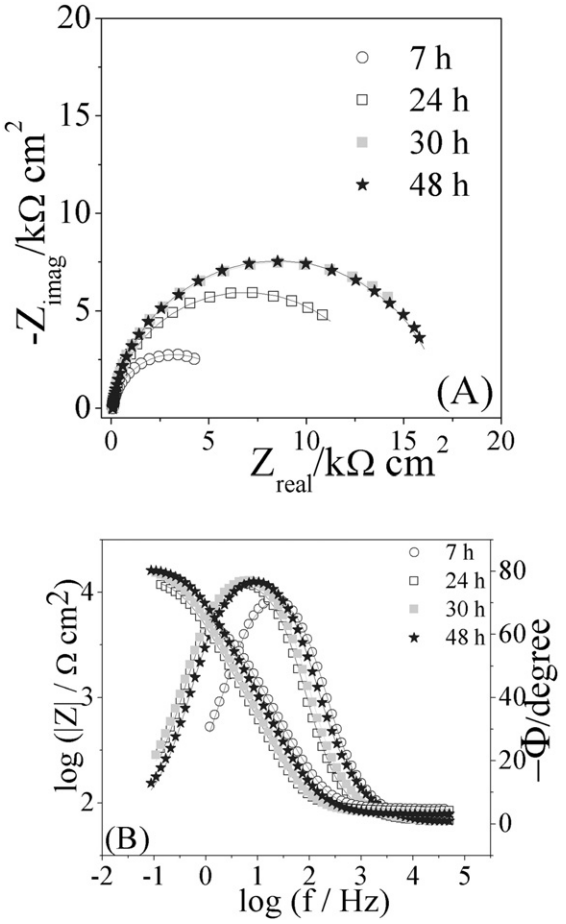

Fig. 11. Experimental (symbols) and fitted (solid lines) EIS diagrams in 0.1 mol l^{-1} NaCl solution for AZ31 alloy protected with the hybrid coating containing 25 mg l^{-1} SiO_2. (A) Nyquist and (B) Bode plots.

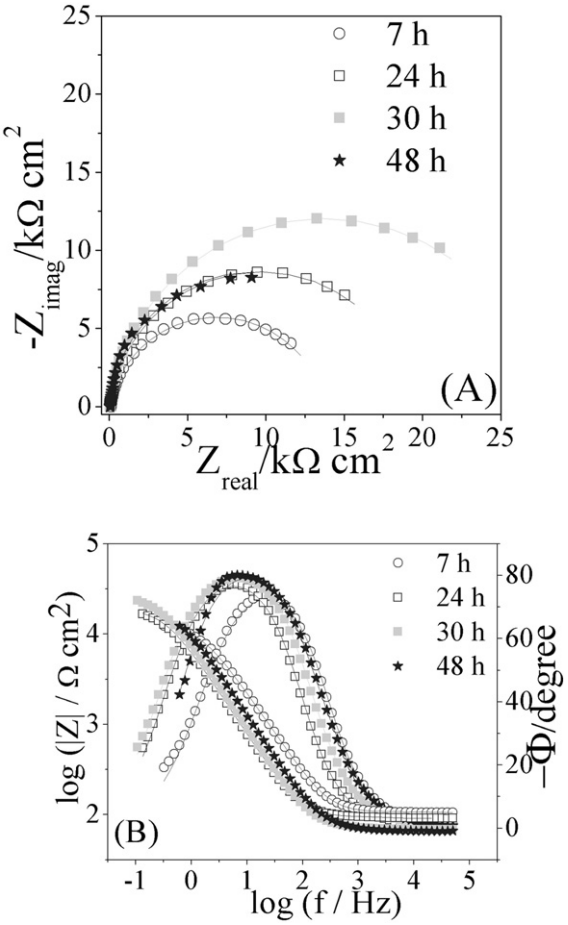

Fig. 12. Experimental (symbols) and fitted (solid lines) EIS diagrams in 0.1 mol l^{-1} NaCl solution for the AZ31 alloy protected with the hybrid coating containing 100 mg l^{-1}SiO_2: (A) Nyquist and (B) Bode plots.

times, so their impedance diagrams will not be presented. After 48 h immersion, the SEM image (Fig. 2(D)) of the coating modified with 400 mg l^{-1} SiO_2 shows the surface similar to that obtained for the one with 300 mg l^{-1}, Fig. 2(C), however cracks seem to be wider. The addition of 600 mg l^{-1} SiO_2 produced a stressed coating with many defects and some cracks, indicating no additional anticorrosion benefit when compared with other coated samples.

Concerning the ability of SiO_2 nanoparticles to improve the anticorrosion performance of coatings, different explanations exist. According to Dolatzadeh *et al.* [55], studying the effect of modified SiO_2 nanoparticles, which resulted in variation of their surface area, the addition of the nanoparticles re-arranges the structure of the coating leading to the improvement of its barrier properties, and consequently, the resistance against corrosion [56]. By studying the protection of carbon steel, Suegama *et al.* [22] stated that the use of bisilanes together with silica nanoparticles enhances the film hardness and the barrier effect of the coating due to thickness increase. Montemor *et al.* [30] demonstrated that the addition of silica particles to silane coatings increased the corrosion protection ability due to the formation of an inner SiO_2 rich-layer (demonstrated by AES depth-profiling) and/or the enhanced barrier properties of the inner layers of the composite coating. In several of these studies, the addition of the SiO_2 nanoparticles to the coatings allowed to increase their impedance compared to the blank coatings [22,30,54,56]. However, from the presented results it seems that the positive effects for the investigated system seems to be effective only at early stages of immersion (up to 30 h depending on the SiO_2 content). For longer immersion times, the continuous electrolyte attack and corrosion propagation on the base material does hinder the beneficial effects of silica addition. An increase of the SiO_2 amount in the coating up to 300 mg l^{-1} improved the coating performance, however, concentrations of 400 and 600 mg l^{-1} SiO_2 made the anticorrosion performance of the coatings decrease, likely due to increased agglomeration. This demonstrates that an optimum amount of nanoparticles must be added to the coating in order to obtain maximum corrosion protection capability, as already verified for other nanoparticle loaded coatings [22,26–28].

4. Conclusions

TEOS- and GPTMS-based hybrid coatings can provide good corrosion protection when applied over AZ31 Mg alloy only for short immersion times in chloride solution. The addition of SiO_2 nanoparticles to the hybrid coating improved the electrochemical response of the system without apparently increasing its lifetime. It was verified that the coating with addition of 100 mg l^{-1} of nanoparticles provided the highest protection during the first hours of immersion in 0.1 mol l^{-1} NaCl, whereas the coating modified with 300 mg l^{-1} SiO_2 showed good corrosion resistance up to 30 h of immersion. Therefore, the maximum amount of SiO_2 nanoparticles that can be added with positive impact on the anticorrosive performance of the hybrid coating must lie within 100 to 300 mg l^{-1} under the conditions of this work.

The application of the hybrid coating seems to improve the anticorrosion performance of the Mg alloy by keeping the corrosion product layer adhered to the metal surface, whereas the addition of the SiO_2 nanoparticles seems to retard the corrosion process as indicated by SEM images and EDS analysis.

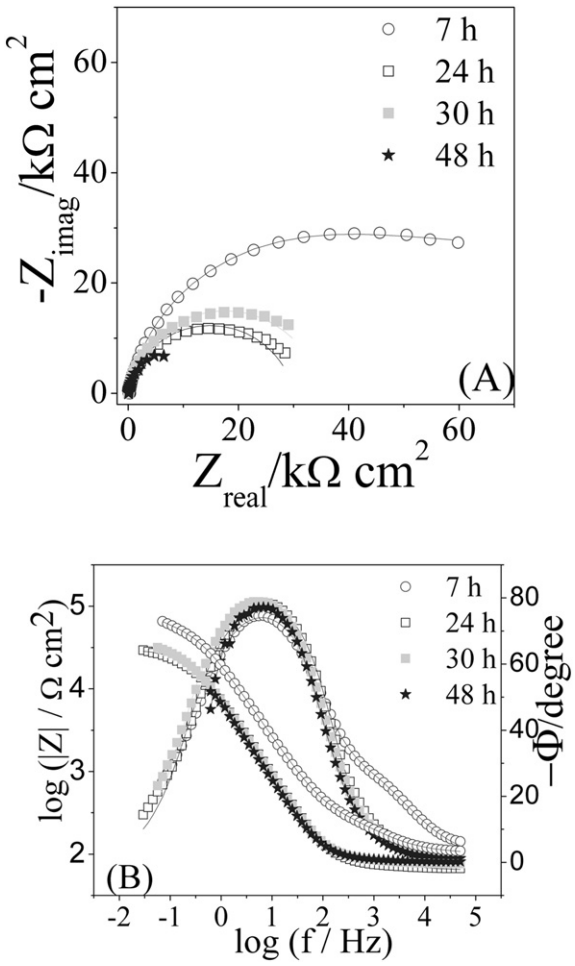

Fig. 13. Experimental (symbols) and fitted (solid lines) EIS diagrams in 0.1 mol l^{-1} NaCl solution for the AZ31 alloy protected with the hybrid coating containing 300 mg l^{-1} SiO_2: (A) Nyquist plots, (B) Bode plots.

Acknowledgments

RNP author acknowledges Universidade Federal da Grande Dourados for the scholarship. AVB author gratefully acknowledges the Brazilian research agency CNPq (Proc. no. 305890/2010-7) for the scholarship. MFM acknowledges Fundação para a Ciência e Tecnologia (FCT) for the funding under the contract UID/QUI/00100/2013. PHS acknowledges FUNDECT for the funding under the process 23/200.693/2012.

References

[1] M. Gupta, N.M.L. Sharon, Magnesium, Magnesium Alloys, and Magnesium Composites, first ed. John Wiley & Sons, Hoboken, 2011.
[2] W.A. Monteiro, New Features on Magnesium Alloys, first ed. InTech, Rijeka, 2012.
[3] R. Pinto, M.J. Carmezim, M.G.S. Ferreira, M.F. Montemor, A two-step surface treatment, combining anodisation and silanisation, for improved corrosion protection of the Mg alloy WE54, Prog. Org. Coat. 69 (2010) 143–149.
[4] C. Sanchez, G.J.D.A.A. Soler-Illia, F. Ribot, D. Grosso, Design of functional nanostructured materials through the use of controlled hybrid organic–inorganic interfaces, C. R. Chim. 6 (2003) 1131–1151.
[5] D. Wang, G.P. Bierwagen, Sol–gel coatings on metals for corrosion protection, Prog. Org. Coat. 64 (2009) 327–338.
[6] F.M.D.L. da Cruz, Estudo eletroquímico de filmes híbridos siloxano – PMMA como pré-tratamentos protetores contra corrosão para aço estanhadoUniv Estadual Paulista, PhD Thesis, Instituto de Química 2013 (140 pp.).
[7] S. Zheng, J. Li, Inorganic–organic sol gel hybrid coatings for corrosion protection of metals, J. Sol–Gel Sci. Technol. 54 (2010) 174–187.
[8] F.A. Carey, Organic Chemistry, seventh ed. Mc Graw-Hill, New York, 2007.
[9] H. Rahimi, R. Mozaffarinia, A.H. Najafabadi, R.S. Razavi, E. Paimozd, Optimization of process factors for the synthesis of advanced chrome-free nanocomposite sol–gel coatings for corrosion protection of marine aluminum alloy AA5083 by design of experiment, Prog. Org. Coat. 76 (2013) 307–317.
[10] K.H. Wu, M.C. Li, C.C. Yang, G.P. Wang, Domain size and thermal stability of amine-cured hybrid films as corrosion resistance treatments for aluminum alloy, J. Non-Cryst. Solids 352 (2006) 2897–2904.
[11] M.L. Zheludkevich, R. Serra, M.F. Montemor, I.M. Miranda Salvado, M.G.S. Ferreira, Corrosion protective properties of nanostructured sol–gel hybrid coatings to AA2024-T3, Surf. Coat. Technol. 200 (2006) 3084–3094.
[12] H. Rahimi, R. Mozaffarinia, A.H. Najafabadi, Corrosion and wear resistance characterization of environmentally friendly sol–gel hybrid nanocomposite coating on AA5083, J. Mater. Sci. Technol. 29 (2013) 603–608.
[13] V.R. Capelossi, M. Poelman, I. Recloux, R.P.B. Hernandez, H.G. de Melo, M.G. Olivier, Corrosion protection of clad 2024 aluminum alloy anodized in tartaric-sulfuric acid bath and protected with hybrid sol–gel coating, Electrochim. Acta 124 (2014) 69–79.
[14] N. Pirhady Tavandashti, S. Sanjabi, T. Shahrabi, Corrosion protection evaluation of silica/epoxy hybrid nanocomposite coatings to AA2024, Prog. Org. Coat. 65 (2009) 182–186.
[15] M.L. Zheludkevich, R. Serra, M.F. Montemor, K.A. Yasakau, I.M. Miranda Salvado, M.G.S. Ferreira, Nanostructured sol–gel coatings doped with cerium nitrate as pre-treatments for AA2024-T3: corrosion protection performance, Electrochim. Acta 51 (2005) 208–217.
[16] X.-H. Guo, M.-Z. An, P.-X. Yang, H.-X. Li, Effect of sol compositions on corrosion protection of SNAP film coated on magnesium alloy, Chin. J. Inorg. Chem. 7 (2009) 1254–1261.
[17] P. Balan, M.J. Shelton, D.O. Li Ching, G. Chuan Han, L.K. Palniandy, Modified silane films for corrosion protection of mild steel, proc. math. sci. 6 (2014) 244–248.
[18] N.C. Rosero-Navarro, S.A. Pellice, A. Duran, M. Aparicio, Effects of Ce-containing sol–gel coatings reinforced with SiO_2 nanoparticles on the protection of AA2024, Corros. Sci. 50 (2008) 1283–1291.
[19] M. Zaharescu, L. Predoana, A. Barau, D. Raps, F. Gammel, N.C. Rosero-Navarro, Y. Castro, A. Durán, M. Aparicio, SiO_2 based hybrid inorganic–organic films doped with TiO_2–CeO_2 nanoparticles for corrosion protection of AA2024 and Mg-AZ31B alloys, Corros. Sci. 51 (2009) 1998–2005.
[20] A. Phanasgaonkar, V.S. Raja, Influence of curing temperature, silica nanoparticles-and cerium on surface morphology and corrosion behaviour of hybrid silane coatings on mild steel, Surf. Coat. Technol. 203 (2009) 2260–2271.
[21] F. Khelifa, M.-E. Druart, Y. Habibi, F. Bénard, P. Leclère, M. Olivier, P. Dubois, Sol–gel incorporation of silica nanofillers for tuning the anti-corrosion protection of acrylate-based coatings, Prog. Org. Coat. 76 (2013) 900–911.
[22] P.H. Suegama, H.G. de Melo, A.A.C. Recco, A.P. Tschiptschin, I.V. Aoki, Corrosion behavior of carbon steel protected with single and bi-layer of silane films filled with silica nanoparticles, Surf. Coat. Technol. 202 (2008) 2850–2858.
[23] D. Del Ángel-López, A.M. Torres-Huerta, M.A. Domínguez-Crespo, E. Onofre-Bustamante, Effect of ZrO_2:SiO_2 dispersion on the thermal stability, mechanical properties and corrosion behavior of hybrid coatings deposited on carbon steel, J. Alloys Compd. 615 (2014) S423–S432.
[24] I. Santana, A. Pepe, E. Jimenez-Pique, S. Pellice, I. Milošev, S. Ceré, Corrosion protection of carbon steel by silica-based hybrid coatings containing cerium salts: effect of silica nanoparticle content, Surf. Coat. Technol. 265 (2015) 106–116.
[25] P.H. Suegama, A.A.C. Recco, A.P. Tschiptschin, I.V. Aoki, Influence of silica nanoparticles added to an organosilane film on carbon steel electrochemical and tribological behaviour, Prog. Org. Coat. 60 (2007) 90–98.
[26] W. Li, H. Tian, B. Hou, Corrosion performance of epoxy coatings modified by nanoparticulate SiO_2, Mater. Corros. 63 (2012) 44–53.
[27] M. Schem, T. Schmidt, J. Gerwann, M. Wittmar, M. Veith, G.E. Thompson, I.S. Molchan, T. Hashimoto, P. Skeldon, A.R. Phani, S. Santucci, M.L. Zheludkevich, CeO_2-filled sol–gel coatings for corrosion protection of AA2024-T3 aluminium alloy, Corros. Sci. 51 (2009) 2304–2315.
[28] F. Ansari, R. Naderi, C. Dehghanian, Improvement in the corrosion resistance of stainless steel 304 L in sodium chloride solution by a nanoclay incorporated silane coating, RSC Adv. 5 (2015) 706–716.
[29] M.A. Silva Alencar, A.V. Benedetti, C.S. Fugivara, Y. Messaddeq, Construção de célula eletroquímica para observação de amostras *in situ* em estereomicroscópio, Quim. Nova 33 (2010) 1394–1397.
[30] M.F. Montemor, A.M. Cabral, M.L. Zheludkevich, M.G.S. Ferreira, The corrosion resistance of hot dip galvanized steel pretreated with Bis-functional silanes modified with microsilica, Surf. Coat. Technol. 200 (2006) 2875–2885.
[31] R.Z. Zand, K. Verbeken, V. Flexer, A. Adriaens, Effects of ceria nanoparticle concentrations on the morphology and corrosion resistance of cerium–silane hybrid coatings on electro-galvanized steel substrates, Mater. Chem. Phys. 145 (2014) 450–460.
[32] G. Baril, N. Pébère, The corrosion of pure magnesium in aerated and deaerated sodium sulphate solutions, Corros. Sci. 43 (2001) 471–484.
[33] G. Galicia, N. Pébère, B. Tribollet, V. Vivier, Local and global electrochemical impedances applied to the corrosion behaviour of an AZ91 magnesium alloy, Corros. Sci. 51 (2009) 1789–1794.
[34] M.F. Montemor, M.G.S. Ferreira, Electrochemical study of modified bis-[triethoxysilylpropyl] tetrasulfide silane films applied on the AZ31 Mg alloy, Electrochim. Acta 52 (2007) 7486–7495.
[35] D.D. MacDonald, Techniques for Characterization of Electrodes and Electrochemical Processes, first ed. John Wiley & Sons, New York, 1991.
[36] R. de Levie, Advances in Electrochemistry and Electrochemical Engineering, first ed. Wiley-Interscience, New York, 1967.
[37] R. de Levie, Fractals and roughelectrodes, J. Electroanal. Chem. 281 (1990) 1–21.
[38] M. Cai, S.-M. Park, Oxidation of zinc in alkaline solutions studied by electrochemical impedance spectroscopy, J. Electrochem. Soc. 143 (1996) 3895–3902.

[39] R. De Levie, On impedance measurements: the determination of the double layer capacitance in the presence of an electrode reaction, Electrochim. Acta 10 (1965) 395–402.
[40] B. Jayaraj, V.H. Desai, C.K. Lee, Y.H. Sohn, Electrochemical impedance spectroscopy of porous ZrO_2-8 wt.% Y_2O_3 and thermally grown oxide on nickel aluminide, Mater. Sci. Eng. 372 (2004) 278–286.
[41] A. Conde, J.J. de Damborenea, Electrochemical impedance spectroscopy for studying the degradation of enamel coatings, Corros. Sci. 44 (2002) 1555–1567.
[42] J.-B. Jorcin, M.E. Orazem, N. Pébère, B. Tribollet, CPE analysis by local electrochemical impedance spectroscopy, Electrochim. Acta 51 (2006) 1473–1479.
[43] G. Baril, G. Galicia, C. Deslouis, N. Pébère, B. Tribollet, V. Vivier, An impedance investigation of the mechanism of pure magnesium corrosion in sodium sulfate solutions, J. Electrochem. Soc. 154 (2007) C108–C113.
[44] F. Mansfeld, Use of Electrochemical Impedance Spectroscopy for the Study of Corrosion Protection by Polymer-Coatings, J. Appl. Electrochem. 25 (1995) 187–202.
[45] J.H. Nordlien, S. Ono, N. Masuko, K. Nisancioglu, Morphology and structure of oxide-films formed on magnesium by exposure to air and water, J. Electrochem. Soc. 142 (1995) 3320–3322.
[46] M. Taheri, M. Danaie, J.R. Kish, TEM examination of the film formed on corroding Mg prior to breakdown, J. Electrochem. Soc. 161 (2014) C89–C94.
[47] M.E. Orazem, B. Tribollet, Electrochemical Impedance Spectroscopy, John Wiley & Sons, New Jersey, 2008.
[48] R. de Levie, The influence of surface roughness of solid electrodes on electrochemical measurements, Electrochim. Acta 10 (1965) 113–130.
[49] R. de Levie, On porous electrodes in electrolyte solutions—IV, Electrochim. Acta 9 (1964) 1231–1245.
[50] V.N. Nguyen, F.X. Perrin, J.L. Vernet, Water permeability of organic/inorganic hybrid coatings prepared by sol–gel method: a comparison between gravimetric and capacitance measurements and evaluation of non-Fickian sorption models, 47 (2005) 397–412.
[51] P. Campestrini, E.P.M. van Westing, J.H.W. de Wit, Influence of surface preparation on performance of chromate conversion coatings on Alclad 2024 aluminum alloy part II: EIS investigation, Electrochim. Acta 46 (2001) 2631–2647.
[52] L.M. Palomino, P.H. Suegama, I.V. Aoki, M.F. Montemor, H.G. De Melo, Electrochemical study of modified cerium–silane bi-layer on Al alloy 2024-T3, Corros. Sci. 51 (2009) 1238–1250.
[53] T. Baskaran, R. Kumaravel, J. Christopher, A. Sakthivel, Silicate anion-stabilized layered magnesium–aluminium hydrotalcite, RSC Adv. 3 (2013) 16392–16398.
[54] V. Palanivel, D. Zhu, W.J. van Ooij, Nanoparticle-filled silane films as chromate replacements for aluminum alloys, Prog. Org. Coat. 47 (2003) 384–392.
[55] F. Dolatzadeh, S. Moradian, M.M. Jalili, Influence of various surface treated silica nanoparticles on the electrochemical properties of SiO_2/polyurethane nanocoatings, Corros. Sci. 53 (2011) 4248–4257.
[56] L. Liu, J.-M. Hu, J.-Q. Zhang, C.-N. Cao, Improving the formation and protective properties of silane films by the combined use of electrodeposition and nanoparticles incorporation, Electrochim. Acta 52 (2006) 538–545.